agriculture

Article

Precise Short-Term Small-Area Sunshine Forecasting for Optimal Seedbed Scheduling in Plant Factories

Liang Gong [1,2], Fei Huang [1], Wei Zhang [1], Yanming Li [1,2,*] and Chengliang Liu [1,2]

[1] School of Mechanical Engineering, Shanghai Jiao Tong University, Shanghai 200240, China; gongliang_mi@sjtu.edu.cn (L.G.); huangfei1999@sjtu.edu.cn (F.H.); zhang_wei@sjtu.edu.cn (W.Z.); chlliu@sjtu.edu.cn (C.L.)

[2] Key Laboratory of Intelligent Agricultural Technology (Yangtze River Delta), Ministry of Agriculture and Rural Affairs, Shanghai 200240, China

* Correspondence: ymli@sjtu.edu.cn

Abstract: Photosynthesis is one of the key issues for vertical cultivation in plant factories, and efficient natural sunlight utilization requires predicting the light falling on each seedbed in a real-time manner. However, public weather services neither provide sunshine data nor meet spatial resolution requirement. Facing these short-term and small-area weather forecasting challenges, we propose a cross-scale approach to infer seedbed-sized areas of sunshine from the city-level public weather services, and then design a seedbed rotation scheduling system for optimal natural sunlight utilization. First, an end-edge-cloud coordinated computing architecture was employed to concurrently aggregate the multi-scale data from weather satellites to sunshine sensors in the plant factory. Second, the small area of sunshine deterministically depends on the meteorological data given a fixed environment, and this correlation was described by a hybrid mapping model, which combined the long short-term memory (LSTM) and gradient boosting decision tree (GBDT) algorithms to form the LSTM-GBDT hybrid prediction algorithm (LGHPA). By training the LGHPA with historical local sensory sunshine and the city-scale meteorological data, the hourly sunshine on a seedbed can be predicted from the public weather forecasting service. Finally, a dynamic seedbed scheduling scheme was constructed to provide uniform solar energy absorption according to the one-hour-ahead radiation estimation. Experiment results show that the hourly sunshine prediction error was less than 18.44% over a seasonal period and the deviation for different solar absorption by seedbeds with rotation capability is less than 7.1%. Consequently, it was demonstrated that the application of short-term, small-area sunshine forecasting improved the performance of seedbed rotation for uniformly absorbed solar radiation. The proposed method verifies the feasibility of precisely predicting small-area sunshine down to the seedbed scale by leveraging a model-based approach and a cloud-edge-end merged cybernetic computing paradigm.

Keywords: end-edge-cloud; machine learning; seedbed rotation; optimal scheduling; regional sunshine prediction

check for updates

Citation: Gong, L.; Huang, F.; Zhang, W.; Li, Y.; Liu, C. Precise Short-Term Small-Area Sunshine Forecasting for Optimal Seedbed Scheduling in Plant Factories. *Agriculture* **2023**, *13*, 1790. https://doi.org/10.3390/agriculture13091790

Academic Editors: Xiuliang Jin, Hao Yang, Zhenhai Li, Changping Huang and Dameng Yin

Received: 10 August 2023
Revised: 5 September 2023
Accepted: 7 September 2023
Published: 9 September 2023

1. Introduction

Plant factories mostly use multi-layered vertical cultivation systems that are suitable for automatic scheduling [1]. The key issue of optimal seedbed rotation scheduling is the regional sunshine forecast down to a 10 m seedbed scale. It is a new fundamental scientific challenge since the goal of most previous research was to predict the weather from minutes to weeks ahead from a temporal perspective. Still, less effort has been made for its spatial counterpart. Existing methods contain some deficiencies when dealing with this emerging issue.

For example, numerical weather prediction (NWP) pertains to solving hydrodynamics and thermodynamics describing the weather evolution process by numerical calculations.

There are difficulties in finding actual conditions of the atmosphere under certain initial and boundary limits, and predicting the atmospheric changes and weather phenomena in a certain future period [2]. Due to the complexity of NWP, a large number of computing resources and dedicated supercomputers are required. This method is usually only used in professional meteorological agencies. Over the years, machine learning (ML) has been widely used in sunshine prediction [3,4]. However, comprehensive ML-based prediction models need large amounts of data for training [5]. Expensive solar illuminometers and advanced meteorological data acquisition systems are only deployed in professional weather services. It is not practical to obtain historical irradiance data for plant factories. On the contrary, the weather forecasting services provided by meteorological agencies are becoming more accurate. Descriptive weather summary and weather forecast data such as temperature, dew temperature, humidity, and wind speed, can be easily obtained from the internet, however, sunshine data is often not available [6]. Moreover, the geographic grid resolution of weather forecasts is about 5 km, which limits its application in a single plant factory. Various research on sunshine forecasting methods has been reported; it can be classified into physical models and statistical methods. Physical models are based on the physical state and dynamic motions of the atmosphere, also known as Numerical Weather Prediction (NWP) models [7], which were believed to be the most appropriate for day-ahead and multi-day forecast horizons [8]. However, NWP models are severely affected by weather factors, such as overcast conditions, cloud evolution, and optical properties in the forecast area [9]. Additionally, the application of such physical models is limited by computational complexity in practical applications [7]. Statistical models are classified into mathematical–statistical models and machine learning algorithms. Mathematical statistical models mainly include regression analysis [10], time series analysis [11], wavelet analysis [12], and others. In practical applications, the prediction accuracy of the mathematical–statistical method is not as high as that of the NWP model due to parameter changes over time. Typical machine learning algorithms include the artificial neural network (ANN) [13], support vector machine (SVM) [14], and heuristic intelligent optimization algorithm [15]. Machine learning does not perform well in long-term prediction. However, it seems to work better for short-term sunshine predictions under unstable sky conditions [9].

The ANN, which is one of the most widely used methods for sunshine prediction, has strong nonlinear function estimation, pattern monitoring, and data sorting ability [16]. Koshy George used feedforward neural networks with a single hidden layer, and presented an online sequential learning algorithm for time series [17]. Yao et al. used and compared BP, GA-BP, and POS-BP neural network algorithms to construct a short-term prediction model for PV output in sunny, cloudy, and rainy weather conditions [18]. ANNs solve a variety of prediction problems and can quickly adapt to various real-world models. However, there are still some shortcomings: (a) a large amount of training data is required for ANNs, and the training duration increases significantly with the increased complexity of the neural network; (b) the reliability of the neural network model depends largely on the topology and parameter selection [19]. A prediction model based on weather classification and SVM was proposed to overcome these limitations. Wang et al. developed a prediction model based on environmental factors and SVM optimized by a genetic algorithm (GA-SVM) to improve the accuracy of short-term power forecasting for PV systems [20]. SVM requires fewer input data compared to ANNs. However, it is hard to train and difficult to handle large-scale training samples. A robust expanded extreme learning machine (EELM) is proposed to accurately predict the solar power for different time horizon and weather condition [21]. A machine learning model based on kernel principal component analysis (PCA)—XGBoost is proposed to improve the accuracy of one-hour-ahead solar power forecasts that achieve good forecasting results for a short-term period [22].

Although ANNs perform excellently in the field of sunshine prediction. It is difficult to fully capture the complex relationships between sunshine and meteorological data, especially temporal relationships. The complex relationships between meteorological data, including linear, nonlinear, and temporal relationships have been analyzed [23].

A comprehensive prediction model for short-term accurate prediction of sunshine was proposed [24]. It uses K-means++ to output different data clusters and establishes a comprehensive prediction model based on LASSO regular regression analysis and LSTM for each data cluster. However, the direct result of classification modeling is that each training process will lose a large amount of effective information, which is extremely unfavorable for the mining of meteorological data. A deep learning model based on LSTM with attention mechanisms is proposed and trained, and results show that the proposed model achieves better results than others but the transformation performed on the data degrades the prediction ability of the models as the representation interval increases [25]. Five machine learning (ML) models which include linear regression, decision tree, random forest, gradient boosting regressor, and support vector regression were evaluated and the results show that gradient boosting performs best with the maximum R2 and decision tree performs best with the minimum MAE and MSE [26]. A deep learning model based on gradient-boosted trees (GBT) was proposed and test results show the minimum estimation error of both RMSE and MAE [27].

In conclusion, research has shown that the hybrid model has high research value and good performance, so we consider constructing a new lighting prediction model according to the advantages and characteristics of different models. Conventionally it is mission impossible to precisely predict hourly sunshine shedding through a greenhouse roof window even with the weather forecast data available. The technical challenges are two-fold. First, we needed to align a measured local sunshine dataflow along with the city weather forecast to establish closely correlated datasets for prediction model training and updates. Meanwhile, a prediction result will be given to the local node for scheduling seedbed rotation in real time. Second, computational architecture was used to reveal the latent time-varying, nonlinear patterns between the local sunshine and the city datasets.

Therefore, to obtain sufficient accuracy and single-day regional sunshine predictions, a sunshine prediction method is proposed here that combines weather forecast data and regional meteorological data. Regional meteorological data of high spatial resolution was added to the acquired professional weather forecast data to correct the deviation between the weather forecast and regional prediction. An optimal seedbed rotation scheduling model was also developed based on the sunshine forecast. The development of sensors, automation equipment and internet of things (IoT) technology has provided feasibility for the intelligent operation of plant factories. We utilized the greenhouse logistics system to implement rotation between two-layer seedbeds.

The optimal seedbed rotation schedule integrates the historical daily sunshine data and regional prediction results, as well as the seedbed station information, and then coordinates the seedbed rotation. The workflow of these robotic services consists of data-hungry, delay-sensitive tasks. Therefore, they were deployed in the end-seedbed control actuator. Generally, the end does not have sufficient computational power and storage capabilities. Tasks in sunshine prediction are usually inter-dependent, data heterogeneous, and computationally intensive. Although existing cloud computing improves computing performance and resource utilization in the centralized computing mode, the centralized transmission of massive data is prone to delay, and users have to directly bear the impact of cloud computing faults [28]. It is thus beneficial to arrange the allocation of computing resources reasonably. A two-layer architecture (cloud-end) can hardly support all the communication and data processing requirements. Then, the scalability, latency, and response time would be affected [29]. Aiming at the above problems, the concept of cloud-edge-end architecture was introduced. Edge computing is an extension of the cloud computing paradigm, providing data, computation, storage, and application services to end-users on a so-called edge layer. It is aware of the combined resource pool composed of both local and virtual resources to facilitate task allocations [30]. The contributions of this research include:

(1) Aiming to solve the uneven distribution of sunshine in plant factory-based stereoscopic cultivation, we propose a novel method that provides uniform sunshine

reception for each seedbed layer by seedbed sequential rotation and establish an optimal seedbed rotation scheduling algorithm (SROSA) based on high-precision sunshine prediction.

(2) To solve the delay-sensitive and computationally intensive coupling problems faced by seedbed scheduling tasks, a cloud-edge-end-based optimal seedbed rotation scheduling architecture is proposed.

(3) For the problem of low spatial resolution in weather forecasts and the lack of sunshine prediction data, the weather forecast data and regional meteorological data are combined to establish the long short-term memory (LSTM) and gradient boosting decision tree (GBDT) hybrid prediction algorithm (LGHPA), to realize high-precision regional prediction.

2. Materials and Methods

This chapter is structured as follows: In Section 2.1, an overview of cloud-edge-end architectures is presented. In Section 2.2, the sunshine prediction model is described. In Section 2.3, the seedbed scheduling model and algorithm are presented.

2.1. Overview of Cloud-Edge-End Architectures

It is practically difficult to forecast the hourly sunshine shedding through a greenhouse roof window because only city-scale data are available from public weather satellites. Therefore, the end-edge-cloud architecture proposed for seedbed scheduling is shown in Figure 1. Plant factories can execute seedbed scheduling tasks according to the calculated sunshine from weather forecast services.

2.1.1. Cloud Computing

In the cloud layer, supercomputers perform complex numerical calculations. In April 2019, China's Meteorological Administration launched a new generation of high-performance computer systems, called Pi ShuGuang, for operational applications. This new system has a computing power of 8189.5 trillion floating-point operations per second and a storage capacity of 23,088 TB. This high-performance computer system has been used in many business and scientific research tasks, including the national high-resolution wind and solar energy multi-source numerical forecasting integration business, global atmospheric reanalysis product development, and many others. In the key areas, the spatial resolution of the weather forecast has reached a grid accuracy of 5 km. Although the cloud carries out complex and huge calculations, it provides many weather-related services for civilian applications. However, long-term sunshine prediction is difficult due to the complicated relationship between sunshine and meteorological, terrestrial, and extraterrestrial variables. Numerical calculations also do not directly provide sunshine prediction at the required spatial scale. Nonetheless, we can use other weather forecast data to complete the construction of our sunshine prediction model by subscribing to free public APIs from the cloud server.

2.1.2. Edge Computing

In the edge computing environment, applications and service functions are placed in edge nodes that can reduce latency and onward network traffic. The service latency can be reduced by placing the applications and service functions near to the end-users. Instead of traversing to the central cloud resources over the high-latency WAN, edge nodes can instantly respond to the user request with minimum network latency [31].

The task of this layer was to perform sunshine prediction calculations and seedbed scheduling decisions. The sunshine prediction model is a computationally intensive, data-hungry task. It obtains the cloud weather forecast data through the weather forecast API and local weather sensor data through communication with the gateway in the END layer. Firstly, we deployed the sunshine prediction model to the plant factory central control server, which created a database that aggregates local and cloud resources. Next, the model acquired the data directly from the database, and the predicted results were transmitted to the seedbed scheduler. The seedbed scheduler is a latency-sensitive application, which needs to continuously acquire local illumination data and illumination predictions to dynamically execute the seedbed scheduling plan. Finally, the scheduling command was sent to the gateway.

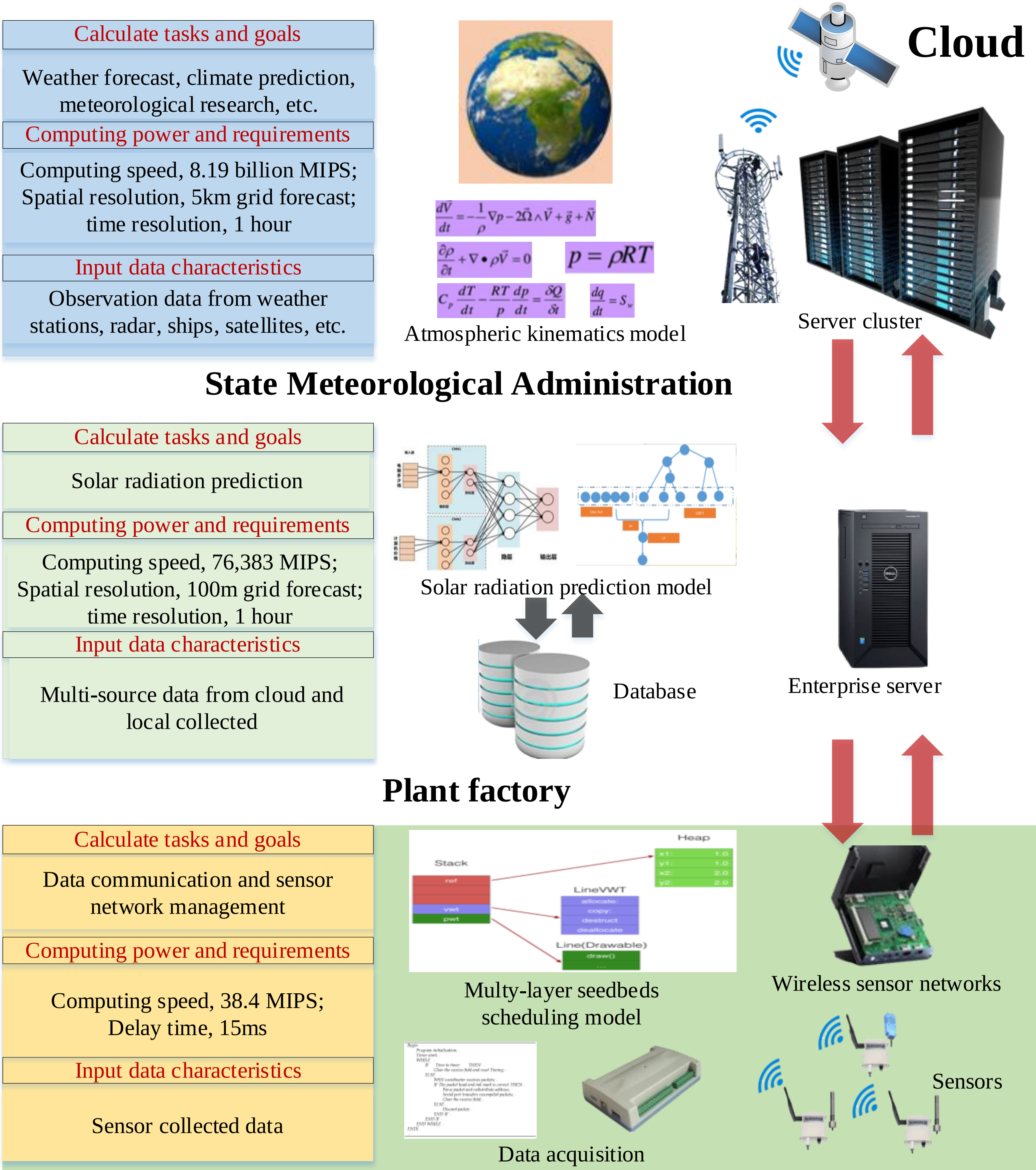

Figure 1. Cloud-edge-end architecture deployment of the seedbed scheduling system.

2.1.3. End Computing

The task of this layer was to collect local meteorological data and transmit it to the edge layer in real time. A sensor network and coordinator (gateway) based on ZigBee wireless technology were deployed in this layer. The goal of the sensor network was to collect meteorological data such as local sunshine intensity, temperature, and humidity, and send it to the gateway at regular intervals. The gateway was responsible for data forwarding to the edge layer and management of the wireless sensor network.

2.2. Sunshine Prediction

We established a comprehensive model that takes into account the linear, nonlinear, and temporal relationships in meteorological and sunshine data. We also used the LSTM algorithm to detect long-term dependencies. LSTM is an improved recurrent neural network (RNN) that solves the problem of gradient disappearance. It has proven to be very successful in mining temporal relationships. Additionally, we used the gradient boosting decision tree (GBDT) to mine implicit relationships in meteorological data. Then, the K-means algorithm was utilized to cluster similar weather data, the weighted average integration was applied to the prediction results of each data cluster, and the optimal weight was found. Finally, the LSTM and GBDT hybrid prediction algorithm (LGHPA) were integrated with LSTM and GBDT without loss of data information, which significantly improved the prediction accuracy.

2.2.1. Data Exploration and Sunshine Model

We collected historical statistical meteorological data from 1990 to 2010 in the Shanghai region of China in the Meteonorm Global Climate Database. It includes 21 meteorological elements such as illumination time, cloud coverage, wind speed, total horizontal radiation, relative humidity, and air pressure. These data were recorded at hourly intervals. At the same time, we obtained hourly weather forecast data for 14 meteorological factors from 20 July 2018 to May 2019 in the plant factory location, Minhang District, Shanghai, via the internet interface. The rest of the data were taken as testing data during this period. We built a wireless sensor network for local data acquisition recording temperature, humidity, and solar radiation every 3 min. Real-time environment data was transmitted to the server through ZigBee wireless sensing technology. The data acquisition platform is shown in Figure 2. We averaged this part of the data in hours to correspond to the timestamps of other meteorological data and added the time feature, month and hour, to the data set. Missing data in datasets were represented by NaN. Solar radiation was labeled as the target, and other meteorological elements were labeled as the $Feature\_ii = 0, 1, \ldots, 38$. We used Python to build and train the model.

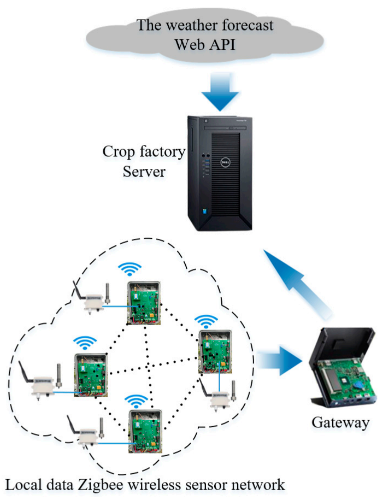

Figure 2. Collection of local data and weather forecast data.

Sunshine is generally considered to be related to meteorological variables such as temperature, humidity, and precipitation. We explored and analyzed the data, results indicate the relationship is very complicated and can be decomposed into the linear relationship, nonlinear relationship, and temporal correlation.

1. Linear component I_A. There are positive and negative correlations between sunshine and some meteorological data, as shown in Figure 3a. The x-coordinate is the time, and the y-coordinate is the equal scale value of each weather element. There is the same or opposite trend between them. The linear relationship between sunshine and meteorological variables is

$$I_A = \theta^T X + \varepsilon, \tag{1}$$

where θ is the parameter vector of the model, including the bias term θ_0 and the feature weights θ_1 to θ_n. θ^T is the transposition vector of θ, X is the weather variable vector, ε is the error term of the linear model.

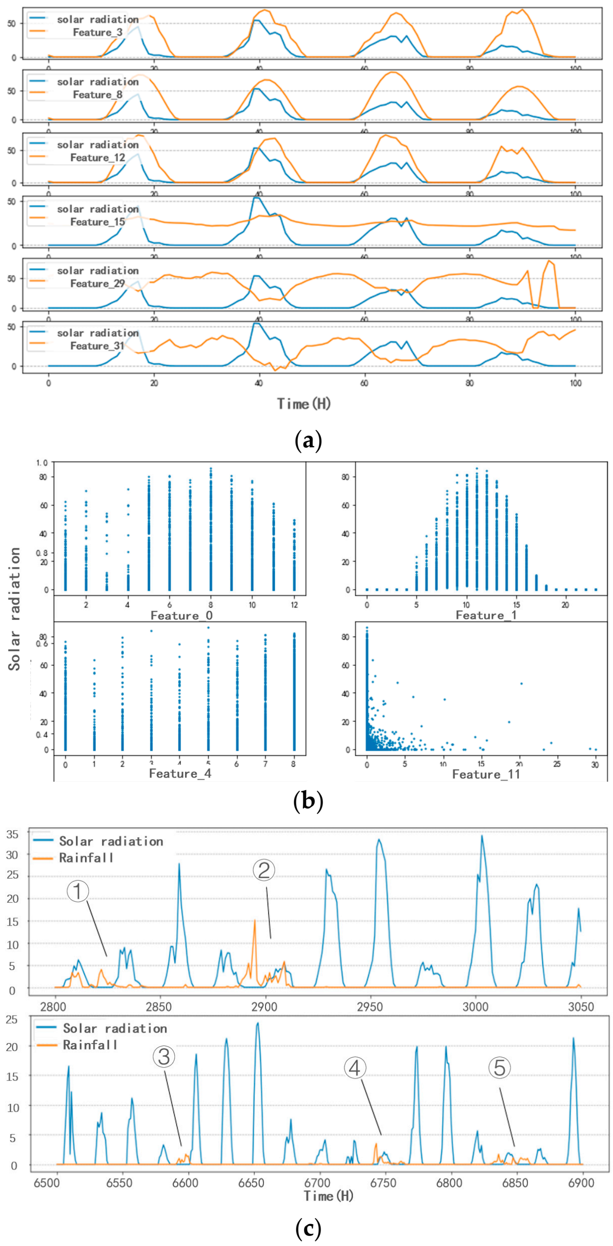

Figure 3. Data exploration and analysis: (**a**) linear relationship; (**b**) nonlinear relationship; (**c**) temporal correlation.

2. Nonlinear component I_B. In Figure 3b, *Feature_0* and *Feature_1* represent the month and hour. It can be seen that sunshine presents a strong seasonality and has a strong regularity in the distribution of the day. The uneven distribution is also presented in *Feature_3* and *Feature_4*. The nonlinear relationship between sunshine and meteorological variables is
$$I_B \sim P(X) + \mu, \tag{2}$$
where $P(\cdot)$ is a nonlinear function, μ is the disturbance term.
3. Temporal components $I(t, \Delta t)$. Meteorological data are often recorded as time series and meteorological characteristics tend to be time-delayed. Figure 3c shows that sunshine always decreases to different degrees before and after rain, and then returns to a strong level some time after rain, as indicated by the mark. The position of the numbers marked in the Figure 3c indicates rainfall here. The temporal correlation between them is
$$I(t, \Delta t) = f(X(t), X(t - \Delta t), \ldots) + \varepsilon(t), \tag{3}$$
4. The comprehensive sunshine model is the integration of the above components
$$I = I_A + I_B + I(t, \Delta t). \tag{4}$$

2.2.2. LSTM and GBDT Hybrid Prediction Algorithm (LGHPA)

According to the data features, we can separately obtain the linear components, nonlinear components and time series components of the meteorological data through the LSTM and GBDT models, where the LSTM unit is a prediction model for inferring temporal components of the solar intensity and GBDT unit is an integrated learning model for estimating the nonlinear and linear components. Then, we combined the prediction results with a weighted average K-means algorithm, which is applied to aggregate weather data clusters of similar weather and chose different weighting coefficients for each cluster. Figure 4 shows the LSTM unit. Figure 5 shows the prediction network model based on LSTM. Figure 6 shows the GBDT model. And Figure 7 shows the general workflow for LGHPA.

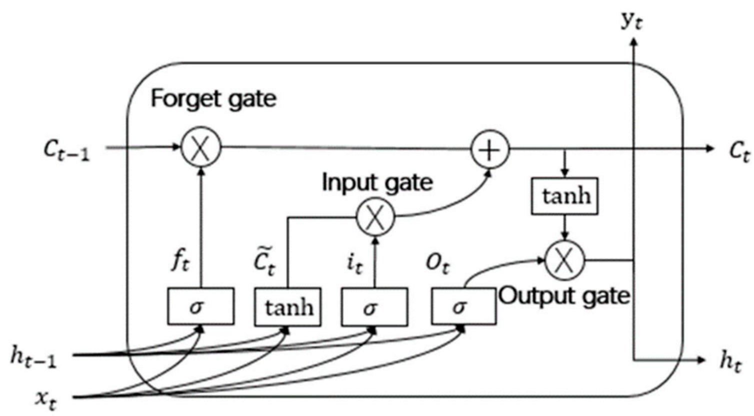

Figure 4. LSTM unit.

First, divide input data into a training set $T = \{X, Y\}_T$ and verification set $E = \{X, Y\}_E$. Then, train the LSTM model to learn the temporal and linear relationships between meteorological data and sunshine. The meteorological data of the previous 48 h were used as an input, and the output was the solar intensity at the current moment. The output results are represented by I_a. Similarly, train the GBDT model to learn the nonlinear relationship, and the output results are represented by I_b. After that, data clustering was performed on the training set $T = \{X, Y\}_T$ using the K-means algorithm. Since the scale of meteorological features is different, if we use the original meteorological data for clustering, the data features with larger scales will have a greater impact on the clustering results.

To make the impact of various meteorological features more balanced, the data was first normalized using Equation (5).

$$x_{scaled} = \frac{x - x_{min}}{x_{max} - x_{min}} \tag{5}$$

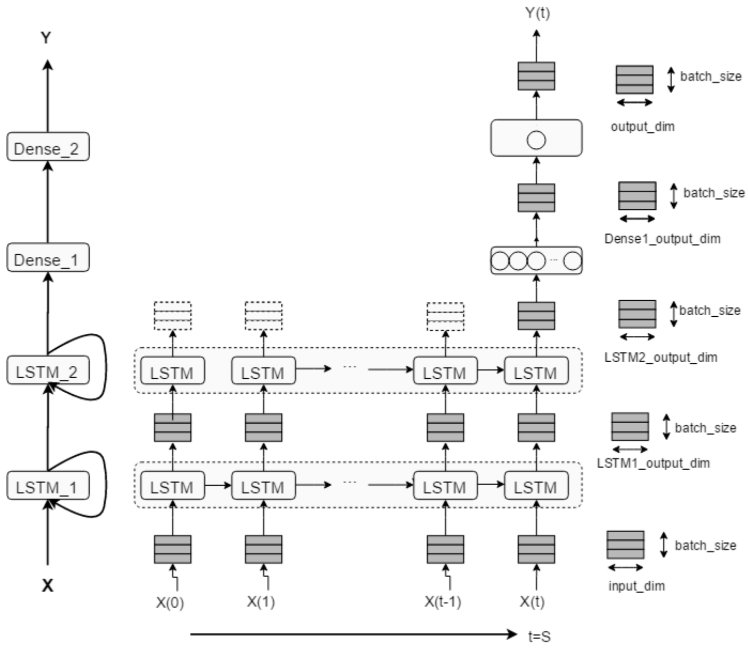

Figure 5. Prediction network model based on LSTM.

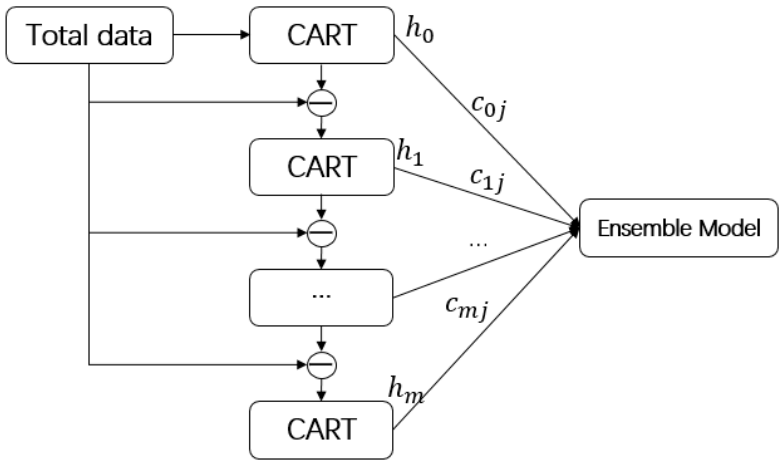

Figure 6. The GBDT model.

Input the normalized data set $T_{scaled} = \{X_{scaled}, Y\}_T$ into the K-means model, and K center points are the output, corresponding to K data clusters. Each sample belongs to one of the data clusters, and the prediction results in the LSTM and GBDT models can also be expressed as $I_a = \{I_{a,1}, \ldots, I_{a,i}, \ldots, I_{a,k}\}$ and $I_b = \{I_{b,1}, \ldots, I_{b,i}, \ldots, I_{b,k}\}$. Finally, calculate the weighted prediction results as follows:

$$\hat{I} = \alpha I_a + (1 - \alpha) I_b \tag{6}$$

where, $\hat{I} = \{\hat{I}_1, \ldots, \hat{I}_i, \ldots, \hat{I}_k\}$ indicates the final prediction result, $\alpha = \{\alpha_1, \ldots, \alpha_i, \ldots, \alpha_K\}$ and $(1 - \alpha)$ represent the weight coefficients of the two models. Figure 7 shows the structure diagram of the LGHPA. We use the traversal method to determine the optimal α_i. The specific implementation is as follows:

1. Initialize $\alpha_i = 0$;
2. Increase the value of α_i gradually until $\alpha_i = 1$, and calculate the root mean square error (RMSE) for each α_i as follows:

$$RMSE_i = \sqrt{\frac{1}{m}\sum_{j=1}^{m}\left(\hat{I_{i,j}} - I_{i,j}\right)^2}, \quad (7)$$

Find the optimal α_i by

$$\alpha_i = argmin\{RMSE_i\}. \quad (8)$$

In this way, we obtain α_i for each data cluster, and we can have all the predicted values by using Equation (6). In the verification process, we first calculated the prediction results of each sample in the verification set using the LSTM and GBDT models, respectively. Then, we classified each data sample into one of the K data clusters. Finally, we found the corresponding weight coefficient to obtain the final predicted value.

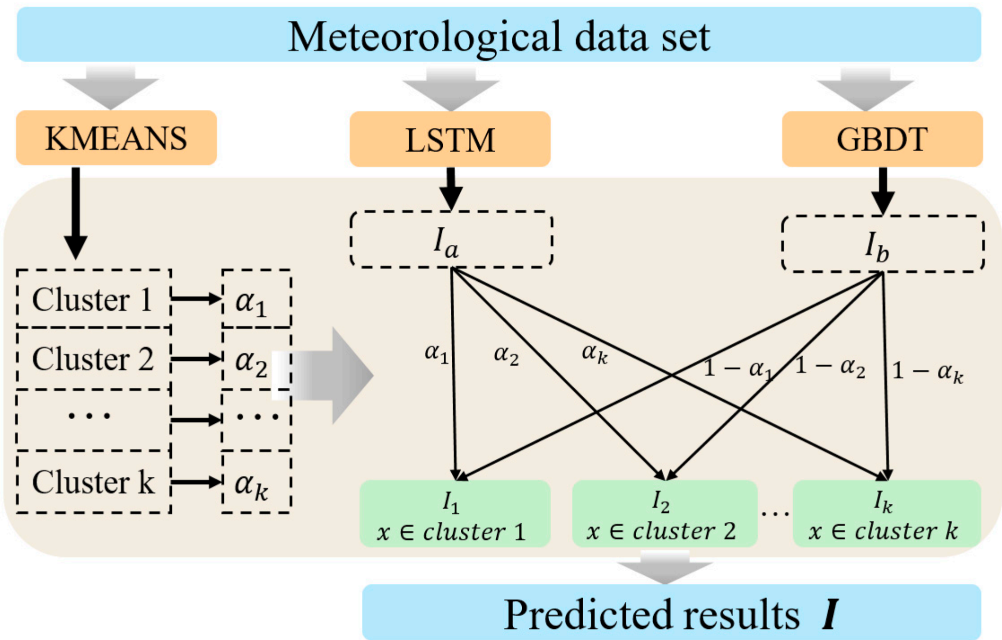

Figure 7. LSTM and GBDT hybrid prediction algorithm (LGHPA).

2.3. *Seedbeds Scheduling Model and Algorithm*

Plants are grown by photosynthesis to produce organic matter. Therefore, the sunshine and illumination time, which directly affect the strength of photosynthesis, have a great influence on the growth and development of plants. In this section, we first analyze the quantity of light model (QoLM) of seedbeds in the multi-layer stereoscopic cultivation and further obtain the optimal seedbed rotation scheduling model. Finally, the scheduling time of the seedbed is determined by the prediction result of the illumination.

2.3.1. Seedbeds Scheduling Model

1. We utilized the quantity of light to measure the sunshine received by seedbeds. The total number of seedbed layers in the multi-layer stereoscopic cultivation was defined as N, and the total number of rotations was P. All the seedbeds were sequentially moved to the top layer to receive the illumination as one rotation. The purpose of the optimal scheduling of seedbed rotation was to determine the time to move to the top layer in the jth rotation of ith seedbed $\vec{T} = T_{i-1,j-1}$, $i \in (1,\ldots,\mathrm{N}), j \in (1,\ldots,\mathrm{P})$, so that the daily quantity of light in seedbeds of each layer were as equal as possible.

The quantity of light, expressed by Q_v, represents the sum of the solar intensity I over a certain period of time, that is

$$Q_v = \int_{T_{start}}^{T_{end}} I(t)dt, \tag{9}$$

where T_{start} indicates the moment when $I(t) \neq 0$ in the day, and T_{end} indicates the moment when there is no more light in the day. $I(t)$ represents the solar intensity in time t.

2. Define the proportion of the quantity of light received by the seedbed in the total quantity of light in the jth rotation as $\vec{c} = (c_0, \ldots, c_{j-1}, \ldots, c_{P-1}), (0 < c_{j-1} \leq 1, \sum_{j=1}^{P} c_{j-1} = 1)$. Then, after the jth rotation, the quantity of light that each layer of the seedbed needs to receive is

$$\vec{X} = \frac{1}{N} \times \vec{c} \times Q, \tag{10}$$

$\vec{X} = (X_0, \ldots, X_{j-1}, \ldots, X_{P-1})$ represents the quantity of light required for each layer of seedbed in the jth rotation.

3. At time t, assuming that the scheduling plan is during the period of the ith rotation. The jth layer seedbed is at the top, then calculating the quantity of light that the ith layer seedbed has received in the jth rotation is calculated as

$$\vec{Q}(t) = \int_{T_{last}}^{t} I(t)dt, \tag{11}$$

T_{last} indicates the latest scheduling time less than time t, indicating the last seedbed scheduling time. $\vec{Q}(t) = Q_{i-1,j-1}(t)$ represent the quantity of light that the ith layer seedbed has received in the jth rotation. $I(t)$ represents the real-time illumination at time t.

4. Calculate the time of seedbed rotation according to Equations (10) and (11),

$$\vec{X} = \vec{Q}(t) + \int_{t}^{T_{next}} I(t)dt, T_{next} == \begin{cases} T_{i,0}, j = P-1 \\ T_{i-1,j}, j < P-1' \end{cases} \tag{12}$$

where T_{next} represents the next seedbed rotation time.

5. In time t, the day sunshine $I(t)$ in Equations (9) and (12) is unknown. To calculate $\vec{T}$, it is necessary to know all the values of $I(t)$ in the day in advance, so it is necessary to predict the solar intensity. Assuming that the predicted sunshine value is $I_{pred}(t)$, then Equations (9) and (12) can be rewritten as

$$Q_v = \int_{T_{start}}^{t} I(t)dt + \int_{t}^{T_{end}} I_{pred}(t)dt, \tag{13}$$

$$\vec{X} = \vec{Q}(t) + \int_{t}^{T_{next}} I_{pred}(t)dt = \int_{T_{last}}^{t} I(t)dt + \int_{t}^{T_{next}} I_{pred}(t)dt. \tag{14}$$

2.3.2. Optimal Seedbed Rotation Scheduling Algorithm (SROSA)

According to the seedbed sunshine analysis and the optimal seedbeds rotation scheduling model in Section A, we propose an optimal seedbed rotation scheduling algorithm (SROSA).

Step 1. Initialize the number of seedbed layers N and the number of rotations P;

Step 2. Initialization start time T_{start} and end time T_{end}, $t = T_{start}, i = 0, j = 0$;

Step 3. Calculate the quantity of light $Q_{i-1,j-1}$(t) that has been received in the j_{th} rotation of the i_{th} layer seedbed according to Equation (11);

Step 4. Calculate the required quantity of light $X_{i-1,j-1}$ in the j_{th} rotation of the i_{th} layer seedbed according to Equation (10) and the predicted sunshine results;

Step 5. Calculate the next scheduling time T_{next} according to Equation (14);

Step 6. $t = t + \Delta t$, then

1. Determine $t \geq T_{end}$. If yes, then end; else, go to step 6.2;
2. Determine $t \geq T_{next}$. If yes, go to step 6.3; else, return to step 3;
3. Determine $i \geq N - 1$. If yes, go to step 6.4; else,. $i = i + 1$, return to step 3;
4. Determine $j \geq P - 1$. If yes, then end; else, $i = 0, j = j + 1$, return to step 3.

3. Results

3.1. Data Description

The datasets are separated into the training datasets and evaluation datasets. Data are stratified by month to ensure the average distribution of data. During the training of GBDT, we found the optimal model parameters for this data set. Table 1 shows the parameters and their optimal values.

Table 1. Parameters of GBDT and their optimal values.

Parameters	Description	Best Value
η	learning rate	0.02
M	number of CART	4617
J	number of leaf nodes in a single CART	30
f_b	bagging fraction	0.4
f_r	feature fraction	0.9

Cross-validation was used in the model test. For each forecast day from July 2018 to March 2019, we used the daily weather forecast and historical data for the previous day to predict the hourly sun radiation value for the day. Then, the sunshine prediction results were input into SROSA. In Section 3.2, we present and analyze the sunshine predictions. In Section 3.3, we present and analyze the seedbed scheduling results.

3.2. Analysis of Sunshine Prediction Results

We tested the performance of the LSTM, the GBDT and LGHPA separately. Then, three performance evaluation criteria, mean absolute error (MAE), normalized mean absolute error (NMAE), and root mean square error (RMSE) were used to test the prediction performance of the proposed forecasting methods.

$$\mathrm{MAE} = \frac{1}{m}\sum_{i=1}^{m}|\hat{y}_i - y_i| \tag{15}$$

$$\mathrm{NMAE} = \frac{\sum_{i=1}^{m}|\hat{y}_i - y_i|}{\sum_{i=1}^{m} y_i} \times 100\% \tag{16}$$

$$\mathrm{RMSE} = \sqrt{\frac{1}{m}\sum_{i=1}^{m}(\hat{y}_i - y_i)^2} \tag{17}$$

We need to determine the value of K in the K-means algorithm when using LGHPA. If K is too big, the complexity of LGHPA will increase and the predictive performance of the model will be sensitive to anomalous data. If the value of K is too small, the prediction accuracy of LGHPA cannot be effectively improved. We tried several values of K. Table 2 shows the comparison of RMSE and MAE, and NMAE of LGHPA when the value of K was at 6–10. According to the table, we can obtain the optimal value for each indicator value of LGHPA when $K = 8$.

So far, we have all the required parameters. The evaluation datasets were input into the LSTM, GBDT, and LGHPA, respectively. The comparison of predicted and observed values is shown in Figure 8. The solid red line indicates that the predicted value is equal to the observed value. Each blue point shows the observed value and the corresponding predicted values at one forecast time. The more intensive the blue point concentrated around the solid red line, the less error between the observed value and predicted value. To be more intuitive, we drew two red dashed lines to represent the two boundaries, within which the absolute error between the predicted value and the observed value is less than 10. Compared to LGHPA, the predicted values of LSTM and GBDT are more scattered outside the boundaries of the two dotted lines. Moreover, some of the predicted values of the LSTM are located on the zero-line. The monthly sunshine average error of the three different algorithms is shown in Figure 9. We can see that the error of LGHPA is mostly smaller than the other two algorithms. The prediction results indicate that the LGHPA is better than the single model.

Table 2. The RMSE and MAE, NMAE of LGHPA (when the value of K is at 6–10).

K	MAE	NAME	RMSE
6	1.641	18.44%	3.710
7	1.634	18.36%	3.701
8	1.633	18.35%	3.695
9	1.635	18.37%	3.713
10	1.638	18.41%	3.711

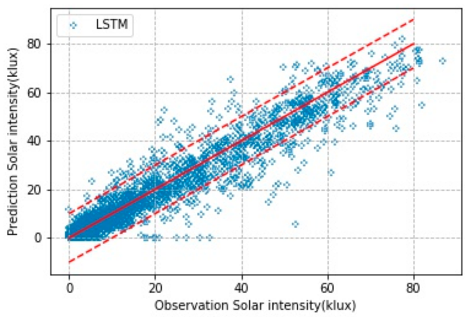

(**a**)

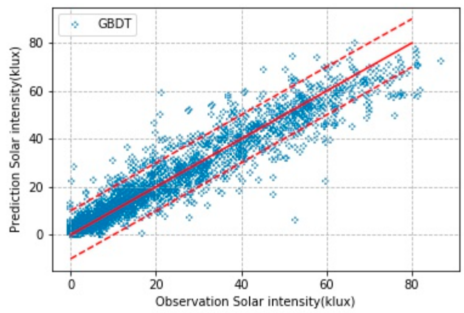

(**b**)

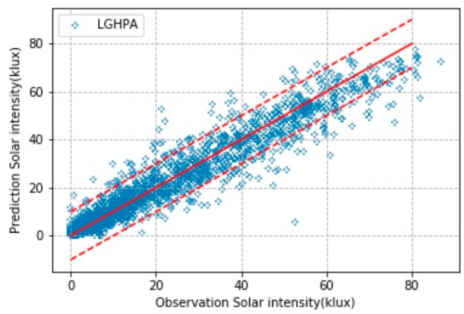

(**c**)

Figure 8. The comparison of predicted and observed values for LSTM, GBDT and LGHPA: (**a**) LSTM; (**b**) GBDT; (**c**) LGHPA.

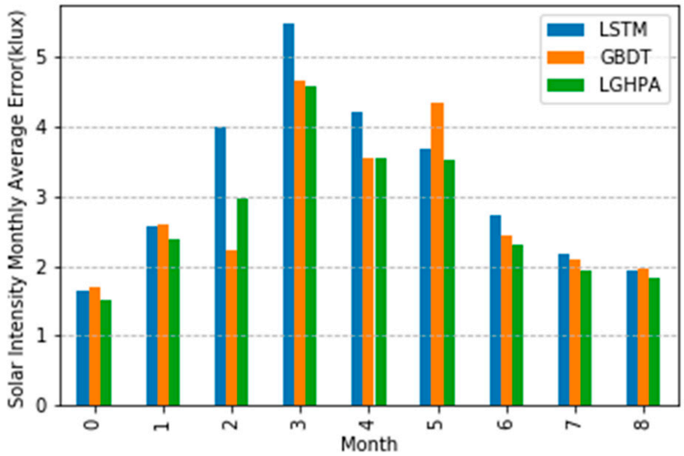

Figure 9. The monthly sunshine average error of LSTM, GBDT and LGHPA.

Table 3 shows the results of MAE, NMAE, and RMSE for the three models. It can be concluded from the table that the prediction accuracy of the GBDT model for sunshine is satisfactory; however, the performance of LSTM is not as good as tha of GBDT. However, by combining LSTM and GBDT according to LGNPA, the prediction accuracy was significantly improved. The MAE, NMAE, and RMSE of LGHPA, compared to the LSTM and GBDT, were reduced by 12.3% and 7.9%, 12.4% and 8.04%, 12.7%, and 9.1%, respectively.

Table 3. Results of MAE, NMAE, and RMSE for LSTM, GBDT, and LGHPA.

Algorithm	MAE	NAME	RMSE
LSTM	1.86	20.9%	4.24
GBDT	1.77	19.9%	4.07
Hybrid	1.63	18.3%	3.70

Table 4 shows the results of MAE, NMAE, RMSE, and nRMSE for the six models, five of which are from the latest research papers. However, the training data set of different models were very different and the performance parameters provided by the paper were different, so it was impossible to achieve qualitative analysis under the same standard, and we could only choose an optimal algorithm to display among the methods compared in the respective paper. At the same time, the time-scale and spatial scale resolution of the LGHPA model proposed in this paper were relatively good, which meets the actual needs of the project.

Table 4. Results of MAE, NMAE, and RMSE for the latest algorithm.

Algorithm	MAE	NAME	RMSE	nRMSE
LGPHA	1.63	18.30%	3.7	-
LSTM-A [25]	NA	NA	84.62	0.253
GBT [27]	5.8212	NA	12.008	NA
GBDT [19]	NA	NA	NA	0.0772
KPCA-XGBoot [22]	NA	NA	14.563	NA
LTSM [6]	NA	NA	76.245	NA

3.3. Analysis of Seedbed Scheduling Results

The schematic diagram of seedbed movement is shown in Figure 10. The shuttle lifts the seedbed and makes a lateral movement on the stereoscopic culture frame. The hoist supports the seedbed for longitudinal movement.

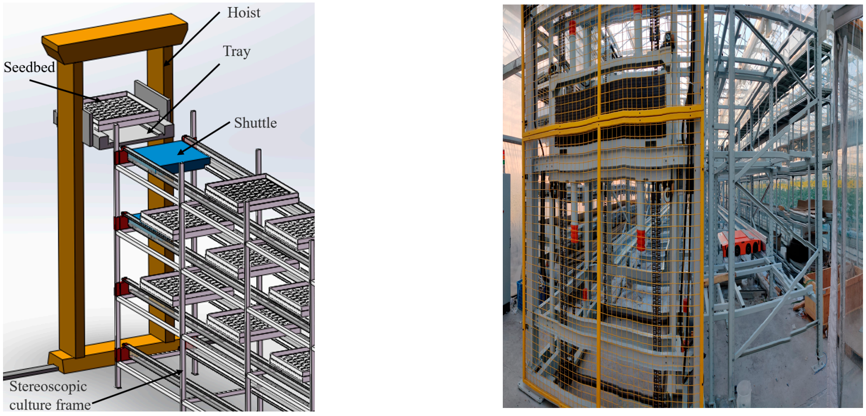

(**a**) (**b**)

Figure 10. The schematic drawing and photograph of seedbed movement routing: (**a**) engineering drawing; (**b**) photograph of multilayer seedbeds.

We input the sunshine prediction results into the SROSA to obtain the scheduling time of the seedbed $\vec{T} = T_{i-1,j-1}$, and further calculated the quantity of light received by the seedbed on the day according to the scheduling time and observation data. The quantity of light received by the N-layer seedbeds during the day is represented by $Q_D = \{Q_1, Q_2, \ldots, Q_N\}$.

$$Q_i = \begin{cases} \sum_{j=1}^{P} \int_{T_{i-2,j-1}}^{T_{i-1,j-1}} I(t)dt \quad i = (2, \ldots, N) \\ \int_{T_{start}}^{T_{0,0}} I(t)dt + \sum_{j=2}^{P} \int_{T_{i-1,j-2}}^{T_{i-1,j-1}} I(t)dt \quad i = 1 \end{cases} \tag{18}$$

We used the daily standard deviation σ_D to test the dispersion of Q_D.

$$\mu_D = \frac{1}{N} \sum_{i=1}^{N} Q_i \tag{19}$$

$$\sigma_D = \sqrt{\frac{1}{N} \sum_{i=1}^{N} (Q_i - \mu_Q)^2} \tag{20}$$

Most multi-layered t stereoscopic cultivation will choose a four-layer structure. Therefore, we set the total number of layers in the seedbed to four and performed a scheduling simulation of 178 forecast days. Figure 11 shows the average daily standard deviation of each algorithm for the number of rotations 1–4. In this figure, the *x*-axis represents the number of rotations, and the three different color histograms represent the average daily standard deviation of the quantity of light falling on the seedbed after the SROSA driven by the three models' prediction results. It can be seen that as the number of rotations increases, the daily standard deviation of the quantity of light received by each layer's seedbed is smaller. In the three prediction models, the LGHPA prediction results can better reduce the difference in the daily average quality of light for the seedbed compared to the other two models. Figure 12 shows the 100-day daily standard deviation of the SROSA results driven by the three models, respectively. The predictions of LSTM and GBDT will make the daily average standard deviation peak more, which is more obvious on the 0th and 48th days. LGHPA eased this situation very well. In practical applications, it is necessary to consider the energy consumption and time cost due to the rotation of the seedbed, so an appropriate number of rotations should be selected.

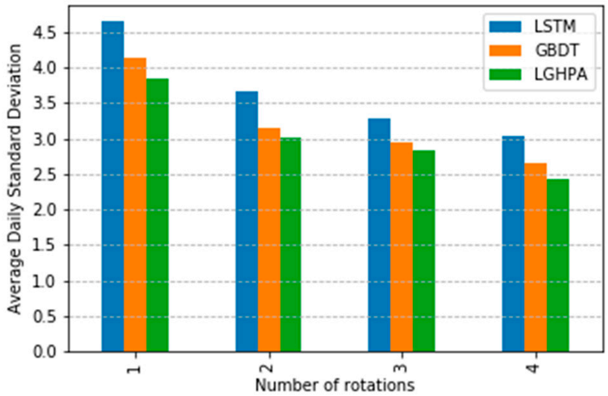

Figure 11. The average daily standard deviation of LSTM, GBDT, and LGHPA for the number of rotations.

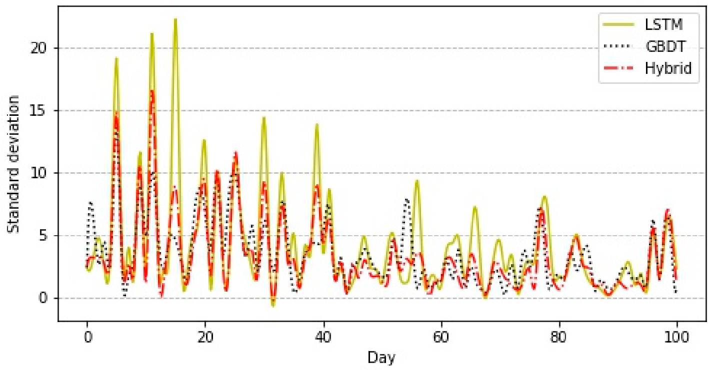

Figure 12. The 100-day daily standard deviation of the SROSA results was driven by three models, respectively.

To prove the effectiveness of SROSA, we gave a lazy seedbed rotation method and made a comparative experiment. The lazy method does not predict sunshine, but only uses historical statistical data to drive the seedbed rotation. Suppose that the historical sunshine data is used to represent the sunshine $I(t)$ of a certain day. Given the known sunshine and assuming that its value does not change over time, we can only perform one rotation. Then, determine the scheduling time $T_S = \{T_0, \ldots, T_i, \ldots, T_N\}$ by

$$Q_S = \frac{1}{N}\int_{T_{start}}^{T_{end}} I(t)dt \tag{21}$$

$$\int_{T_{start}}^{T_0} I(t)dt = \int_{T_{i-2}}^{T_{i-1}} I(t)dt = Q_S \tag{22}$$

In the lazy method, the coefficient of variation CV is used to represent the dispersion of the quantity of light received by seedbeds in a day, that is

$$\mathrm{CV} = \frac{\sigma_D}{\mu_D} * 100\% \tag{23}$$

Figure 13 shows the 175-day coefficient of variation of the quantity of light received by the seedbeds for the lazy method and the SROSA, the dispersion of the amount of light received by the seedbed is much smaller than that of the lazy method. We calculated the average coefficient of variation for all predicted days. The average coefficient of variation by the SROSA method was reduced by about five times compared to the lazy method, which were 7.1% and 35.1%.

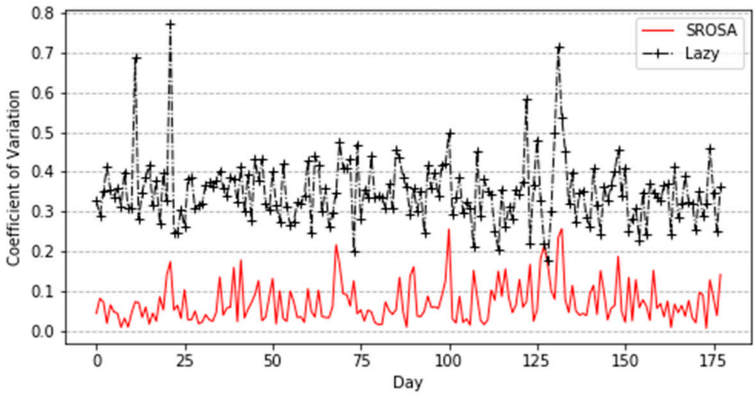

Figure 13. The 175-day coefficient of variation of quantity of light received by seedbeds for the lazy method and the SROSA.

In general, the proposed sunshine prediction approach using LGHPA outperforms the conventional weather prediction counterpart in terms of its spatial resolution, which estimates the seedbed-sized sunshine with over 85% accuracy. Accordingly, the derived seed rotation efficiency is improved by over 30 percent.

4. Discussion

In this paper, we presented a seedbed rotation scheduling system applied to stereoscopic cultivation in plant factories.

Aiming to solve the uneven distribution of sunshine in plant factory-based stereoscopic cultivation, we proposed a novel method that provides uniform sunshine reception for each seedbed layer by sequential seedbed rotation and establishes an optimal seedbed rotation scheduling algorithm (SROSA) based on high-precision sunshine prediction.

To solve the delay-sensitive and computationally intensive coupling problems faced by seedbed scheduling tasks, a cloud-edge-end-based optimal seedbed rotation scheduling architecture was proposed.

For the problem of low spatial resolution in weather forecasting and the lack of sunshine prediction data, the weather forecast data and regional meteorological data were combined to establish the long short-term memory (LSTM) and gradient boosting decision tree (GBDT) hybrid prediction algorithm (LGHPA), to realize high precision regional prediction.

For each forecast day from July 2018 to March 2019, we used the daily weather forecast and historical data for the previous day to predict the hourly sun radiation value for the day. Then, the sunshine prediction results were input into SROSA. We tested the performance of the LSTM, the GBDT, and LGHPA separately. Results show that the error of LGHPA is mostly smaller than the other two algorithms. The prediction results indicate that the LGHPA is better than the single model. The MAE, NMAE, and RMSE of LGHPA, compared to the LSTM and GBDT, were reduced by 12.3% and 7.9%, 12.4% and 8.04%, 12.7%, and 9.1%, respectively, which means that the combination of GBDT and LSTM is feasible and effective. Then, we input the sunshine prediction results into the SROSA to obtain the scheduling time for the seedbed and further calculated the quantity of light. Results show that the LGHPA prediction results can better reduce the daily average difference for the quantity of light falling on the seedbed compared with the other two models.

At present, due to the high procurement costs for historical weather data and limitations of time and equipment, the data collected in this subject for the prediction of optical radiation intensity is only one year old. And the types of data collected are relatively small. And sunshine prediction at each geographic location point requires the model to be retrained. Therefore, it is necessary to study incremental learning and model updating in online data. Additionally, we plan to expand the dataset to optimize the prediction model, collecting more real-time weather data to further improve prediction accuracy, and add local lighting sensors, compare prediction data with measured data, and continuously improve the accuracy of prediction models incrementally.

5. Conclusions

This paper has presented a seedbed rotation scheduling system applied to stereoscopic cultivation in plant factories. According to its latency-sensitive, data-hungry and computationally intensive characteristics, we proposed cloud-edge-end-coordinated computing of the seedbed scheduling system deployment architecture to meet its delay-sensitive and context-aware service requirements. Firstly, we established a comprehensive model that takes into account the linear, nonlinear and temporal relationships in meteorological data and sunshine intensity. We utilized the LSTM algorithm to detect long-term dependencies. and applied GBDT to mine implicit relationships in meteorological data. The K-means algorithm was employed to cluster similar weather features, the weighted average integration was applied to the prediction results of each data cluster, and the optimal weight was obtained. The LGHPA was used to integrate LSTM and GBDT without loss of data information, which significantly improves the prediction accuracy. Then, we established SROSA based on predicted sunshine intensity, according to the multi-layered cultivation characteristics. Finally, we implemented the simulation evaluation of the proposed LGHPA and SROSA. The results show that the MAE, NMAE, and RMSE, of LGHPA, compared to the LSTM and GBDT, were reduced by 12.3% and 7.9%, 12.4% and 8.04%, 12.7%, and 9.1%, respectively. The average coefficient of variation by the SROSA method was reduced by about five times compared to the lazy method, which were 7.1% and 35.1%. The LGHPA can be improved to predict sunshine at different time scales and is also applicable in other scenarios rather than being limited to plant factories.

Author Contributions: Conceptualization, L.G.; methodology, L.G.; software, L.G. and F.H.; investigation, L.G., F.H. and W.Z.; resources, Y.L.; visualization, L.G. and F.H.; validation, F.H., W.Z. and L.G., writing—original draft preparation, F.H. and L.G.; writing—review and editing, L.G., F.H. and Y.L.; supervision, L.G., Y.L. and C.L.; project administration, Y.L. and C.L.; funding acquisition, Y.L. All authors have read and agreed to the published version of the manuscript.

Funding: This work was supported by the 2020 Shanghai "Science and Technology Innovation Action Plan" Agricultural Field Program (grant number 20392000900).

Institutional Review Board Statement: Not applicable.

Data Availability Statement: The data presented in this study are available on request from the corresponding author. The data are not publicly available due to the privacy.

Conflicts of Interest: The authors declare no conflict of interest. The funders had no role in the design of the study; in the collection, analyses, or interpretation of data; in the writing of the manuscript, or in the decision to publish the results.

References

1. Zhang, X.; Zhou, Z.; Wang, J. Research and application of the plant factory key technologies. *North. Hortic.* **2010**, *4*, 204–207.
2. Diagne, M.; David, M.; Lauret, P.; Boland, J.; Schmutz, N. Review of Solar Irradiance Forecasting Methods and a Proposition for Small-Scale Insular Grids. *Renew. Sustain. Energy Rev.* **2013**, *27*, 65–76. [CrossRef]
3. Bae, K.Y.; Jang, H.S.; Sung, D.K. Hourly Solar Irradiance Prediction Based on Support Vector Machine and Its Error Analysis. *IEEE Trans. Power Syst.* **2017**, *32*, 935–945. [CrossRef]
4. Ceci, M.; Corizzo, R.; Fumarola, F.; Malerba, D.; Rashkovska, A. Predictive Modeling of PV Energy Production: How to Set Up the Learning Task for a Better Prediction? *IEEE Trans. Ind. Inform.* **2017**, *13*, 956–966. [CrossRef]
5. Zhang, X.; Li, Y.; Lu, S.; Hamann, H.F.; Hodge, B.-M.; Lehman, B. A Solar Time Based Analog Ensemble Method for Regional Solar Power Forecasting. *IEEE Trans. Sustain. Energy* **2019**, *10*, 268–279. [CrossRef]
6. Qing, X.; Niu, Y. Hourly Day-Ahead Solar Irradiance Prediction Using Weather Forecasts by LSTM. *Energy* **2018**, *148*, 461–468. [CrossRef]
7. Wang, S.-Y.; Qiu, J.; Fang-Fang, L. Hybrid Decomposition-Reconfiguration Models for Long-Term Solar Radiation Prediction Only Using Historical Radiation Records. *Energies* **2018**, *11*, 1376. [CrossRef]

8. Perez, R.; Lorenz, E.; Pelland, S.; Beauharnois, M.; Van Knowe, G.; Hemker, K.; Heinemann, D.; Remund, J.; Müller, S.C.; Traunmüller, W.; et al. Comparison of Numerical Weather Prediction Solar Irradiance Forecasts in the US, Canada and Europe. *Sol. Energy* **2013**, *94*, 305–326. [CrossRef]
9. Mathiesen, P.; Collier, C.; Kleissl, J. A High-Resolution, Cloud-Assimilating Numerical Weather Prediction Model for Solar Irradiance Forecasting. *Sol. Energy* **2013**, *92*, 47–61. [CrossRef]
10. Trapero, J.R.; Kourentzes, N.; Martin, A. Short-Term Solar Irradiation Forecasting Based on Dynamic Harmonic Regression. *Energy* **2015**, *84*, 289–295. [CrossRef]
11. Voyant, C.; Paoli, C.; Muselli, M.; Nivet, M.-L. Multi-Horizon Solar Radiation Forecasting for Mediterranean Locations Using Time Series Models. *Renew. Sustain. Energy Rev.* **2013**, *28*, 44–52. [CrossRef]
12. Akarslan, E.; Hocaoğlu, F.O.; Edizkan, R. A Novel M-D (Multi-Dimensional) Linear Prediction Filter Approach for Hourly Solar Radiation Forecasting. *Energy* **2014**, *73*, 978–986. [CrossRef]
13. Sharifi, S.S.; Rezaverdinejad, V.; Nourani, V. Estimation of Daily Global Solar Radiation Using Wavelet Regression, ANN, GEP and Empirical Models: A Comparative Study of Selected Temperature-Based Approaches. *J. Atmos. Sol. Terr. Phys.* **2016**, *149*, 131–145. [CrossRef]
14. Lauret, P.; Voyant, C.; Soubdhan, T.; David, M.; Poggi, P. A Benchmarking of Machine Learning Techniques for Solar Radiation Forecasting in an Insular Context. *Sol. Energy* **2015**, *112*, 446–457. [CrossRef]
15. Wang, J.; Jiang, H.; Wu, Y.; Dong, Y. Forecasting Solar Radiation Using an Optimized Hybrid Model by Cuckoo Search Algorithm. *Energy* **2015**, *81*, 627–644. [CrossRef]
16. Voyant, C.; Notton, G.; Kalogirou, S.; Nivet, M.-L.; Paoli, C.; Motte, F.; Fouilloy, A. Machine Learning Methods for Solar Radiation Forecasting: A Review. *Renew. Energy* **2017**, *105*, 569–582. [CrossRef]
17. George, K.; Mutalik, P. A Multiple Model Approach to Time-Series Prediction Using an Online Sequential Learning Algorithm. *IEEE Trans. Syst. Man Cybern. Syst.* **2019**, *49*, 976–990. [CrossRef]
18. Yao, Z.; Pan, F.; Shen, Y. Short-term Prediction of Photovoltaic Power Generation Output Based on GA-BP and POS-BP Neural Network. *Power Syst. Prot. Control* **2015**, *43*, 83–89.
19. Wang, J.; Li, P.; Ran, R.; Che, Y.; Zhou, Y. A Short-Term Photovoltaic Power Prediction Model Based on the Gradient Boost Decision Tree. *Appl. Sci.* **2018**, *8*, 689. [CrossRef]
20. Wang, J.; Ran, R.; Song, Z.; Sun, J. Short-Term Photovoltaic Power Generation Forecasting Based on Environmental Factors and GA-SVM. *J. Electr. Eng. Technol.* **2017**, *12*, 64–71. [CrossRef]
21. Mishra, S.; Tripathy, L.; Satapathy, P.; Dash, P.K.; Sahani, N. An Efficient Machine Learning Approach for Accurate Short Term Solar Power Prediction. In Proceedings of the 2020 International Conference on Computational Intelligence for Smart Power System and Sustainable Energy (CISPSSE), Keonjhar, India, 29–31 July 2020; pp. 1–6.
22. Phan, Q.-T.; Wu, Y.-K.; Phan, Q.-D. Short-Term Solar Power Forecasting Using XGBoost with Numerical Weather Prediction. In Proceedings of the 2021 IEEE International Future Energy Electronics Conference (IFEEC), Taipei, Taiwan, 16–19 November 2021; pp. 1–6.
23. Wang, Y.; Shen, Y.; Mao, S.; Cao, G.; Nelms, R.M. Adaptive Learning Hybrid Model for Solar Intensity Forecasting. *IEEE Trans. Ind. Inform.* **2018**, *14*, 1635–1645. [CrossRef]
24. Wang, Y.; Shen, Y.; Mao, S.; Chen, X.; Zou, H. LASSO and LSTM Integrated Temporal Model for Short-Term Solar Intensity Forecasting. *IEEE Internet Things J.* **2019**, *6*, 2933–2944. [CrossRef]
25. Cesar, L.B.; Angel Manso Callejo, M.; Cira, C.-I. Two Novel Deep Learning Models for Short-term Forecasting of Solar Radiation Using Meteorological Variables. In Proceedings of the 2022 17th Iberian Conference on Information Systems and Technologies (CISTI), Madrid, Spain, 22–25 June 2022; pp. 1–6.
26. Varughese, R.A.; Karpagam, R. Prediction Of Solar Power Generation Based On Machine Learning Algorithm. In Proceedings of the 2022 Third International Conference on Intelligent Computing Instrumentation and Control Technologies (ICICICT), Kannur, India, 11–12 August 2022; pp. 396–400.
27. Sepideh Hassankhani, D.; Budinska, I.; Balogh, Z.; Moizis, J.; Saeid Hassankhani, D. Prediction of Photovoltaic Energy Production Using Machine Learning Methods in the RapidMiner Application. In Proceedings of the 2022 IEEE 26th International Conference on Intelligent Engineering Systems (INES), Crete, Greece, 12–15 August 2022; pp. 21–26.
28. Khan, W.Z.; Ahmed, E.; Hakak, S.; Yaqoob, I.; Ahmed, A. Edge Computing: A Survey. *Future Gener. Comput. Syst.* **2019**, *97*, 219–235. [CrossRef]
29. Bellavista, P.; Berrocal, J.; Corradi, A.; Das, S.K.; Foschini, L.; Zanni, A. A Survey on Fog Computing for the Internet of Things. *Pervasive Mob. Comput.* **2019**, *52*, 71–99. [CrossRef]
30. Afrin, M.; Jin, J.; Rahman, A.; Tian, Y.-C.; Kulkarni, A. Multi-Objective Resource Allocation for Edge Cloud Based Robotic Workflow in Smart Factory. *Future Gener. Comput. Syst.* **2019**, *97*, 119–130. [CrossRef]
31. Son, J.; Buyya, R. Latency-Aware Virtualized Network Function Provisioning for Distributed Edge Clouds. *J. Syst. Softw.* **2019**, *152*, 24–31. [CrossRef]